

DeepTheft: Stealing DNN Model Architectures through Power Side Channel

Yansong Gao^{*}, Huming Qiu[†], Zhi Zhang[‡], Binghui Wang[§],
Hua Ma[¶], Alsharif Abuadbba^{*}, Minhui Xue^{*}, Anmin Fu^{||}, Surya Nepal^{*}

^{*}CSIRO's Data61 [†]Fudan University [‡]The University of Western Australia

[§]Illinois Institute of Technology ^{||}Nanjing University of Science and Technology [¶]The University of Adelaide

Abstract—Deep Neural Network (DNN) models are often deployed in resource-sharing clouds as Machine Learning as a Service (MLaaS) to provide inference services. To steal model architectures that are of valuable intellectual properties, a class of attacks has been proposed via different side-channel leakage, posing a serious security challenge to MLaaS.

Also targeting MLaaS, we propose a new end-to-end attack, DeepTheft, to accurately recover complex DNN model architectures on general processors via the RAPL (Running Average Power Limit)-based power side channel. While unprivileged access to the RAPL has been disabled in bare-metal OSes, we observe that the RAPL is still legitimately accessible in a platform as a service, e.g., the latest docker environment of version 20.10.18 used in this work. However, an attacker can acquire only a low sampling rate (1 KHz) of the time-series energy traces from the RAPL interface, rendering existing techniques ineffective in stealing large and deep DNN models. To this end, we design a novel and generic learning-based framework consisting of a set of meta-models, based on which DeepTheft is demonstrated to have high accuracy in recovering a large number (thousands) of models architectures from different model families including the deepest ResNet152. Particularly, DeepTheft has achieved a Levenshtein Distance Accuracy of 99.75% in recovering network structures, and a weighted average F1 score of 99.60% in recovering diverse layer-wise hyperparameters. Besides, our proposed learning framework is general to other time-series side-channel signals. To validate its generalization, another existing side channel is exploited, i.e., CPU frequency. Different from RAPL, CPU frequency is accessible to unprivileged users in bare-metal OSes. By using our generic learning framework trained against CPU frequency traces, DeepTheft has shown similarly high attack performance in stealing model architectures.

1. Introduction

Recent years have witnessed a huge success of Deep Neural Networks (DNN) in various areas, e.g., pattern recognition, computer vision, and natural language processing. Generally, DNN models are often deployed in resource-sharing clouds to provide inference service, also called

Machine Learning as a Service (MLaaS) [2], [17]. A key factor determining a DNN's performance is its model architecture (i.e., comprised of DNN layer type and layer-wise hyperparameters), which is carefully designed via substantial human intelligence and intensive computing resources. Thus, DNNs' model architectures are regarded as valuable intellectual properties and high-value targets to an adversary [46], [50]. Additionally, a known DNN architecture can also be a premise to take further attacks such as model weights stealing [32], model hyperparameter stealing [44], membership inference [8], [38], property inference [14], and data reconstruction [6], [13].

Side-Channel DNN Model Architecture Stealing: A number of works [7], [10], [23]–[25], [28]–[30], [46], [48]–[51], [54], [56] have been proposed to steal DNN model architectures based on different side-channel leakage (e.g., power [10], [29], [48], [49], [54], Electromagnetic (EM) emanations [7], [25], [28], [51], cache [50]).

These attacks can be classified into two categories. One category requires physical proximity or access to target machines hosting victim models [7], [10], [23]–[25], [28], [48], [49], [51], [56] as they need specialized equipment (e.g., magnetic sensors) to collect physical side-channel traces (e.g., magnetic signals) from target machines. In this category, some attacks [7], [24] aim to steal shallow DNN models (fewer than 20 layers) running on edge devices (e.g., microprocessors) while others [23], [28] focus on attaining complex DNN models on advanced hardware (e.g., high-performance GPU).

The other category of attacks avoids the above requirement, where an attacker can co-reside with the same physical machine with victim models [46], [50], thus posing a more significant threat to the MLaaS. In this category, almost all attacks target advanced hardware, as they are widely used in resource-sharing clouds. In this MLaaS setting, Cache Telepathy [50] is the only attack that infers a DNN model on general x86 CPUs via a cache side channel, as general processors are widely used by cloud platforms for model inference services [3], [21]. Please note that general CPUs are supported by cloud providers for model inference because their optimal cost-efficiency, e.g., AWS [3], Google [16] and Alibaba Clouds [1] all supporting CPU inference. In the same setting [50], we ask the following research question:

Yansong Gao. Email: gao.yansong@hotmail.com

Zhi Zhang is the corresponding author. Email: zhi.zhang@uwa.edu.au

Is it feasible to leverage other side channel(s) on general CPUs to accurately and stealthily steal complex DNN architectures with legitimate system access?

DeepTheft: In this paper, we provide an affirmative answer to the question. We propose a new side-channel-based model architecture stealing attack, called DeepTheft, which targets x86 CPUs in the MLaaS. Orthogonal to the cache side channel [50], DeepTheft exploits RAPL (Running Average Power Limit)-based power side channel [26], [27], for the first time, to perform the model architecture stealing. Note that DeepTheft is a stepping stone to weight stealing attacks either through side-channel [32] or queried-based [31], which requires white-box knowledge of model architecture, especially for commonly used complex/deep models.

The RAPL is provided by Intel [27] or AMD processors [26] as power management for software and has been widely used in clouds [20], [37], [52]. Particularly, leveraging this power side channel enables an attacker to passively (i.e., being stealthy) collect energy-consumption traces when a DNN model is performing inferences. We note that although access to the RAPL interface has been restricted to privileged software in the bare-metal OS setting, it is still accessible in the cloud setting. Particularly, we show that an attacker inside a container still has access to the RAPL interface and thus can read out the energy consumption of the system in the latest docker environment of 20.10.18, which is a prevalent containerization platform in practice [11], e.g., it has been commercialized by Amazon to deploy DNN models for model inference services [4]. Also, we have experimentally confirmed that an attacker with a VM-privilege can extract power consumption through RAPL MSR in the commercial cloud of AWS (e.g., an EC2 instance type of c4.8xlarge).

DeepTheft is motivated by [27] that discovered the RAPL-based power side-channel on x86 processors, presenting a common characteristic with previous representative works (e.g., Cache Telepathy [50] in USENIX SEC'20 and DeepSteal [32] in Oakland'22), that is, all these works do not discover a side channel and they instead exploit an existing side channel to break the data confidentiality of deep learning. Particularly for DeepTheft, it is demonstrated to exploit the RAPL side channel to steal large and deep model architectures. To the best of our knowledge, the state-of-the-art (SOTA) side-channel attack [28] is the only existing one that steals full model architectures of 64 large and deep networks, which are prevalent in practice (e.g., ResNet101 [22]). While the SOTA requires physical proximity and a specialized probe to sample EM signals from a target high-end GPU at a rate of no less than 47 KHz, it is also a learning-based approach. We thus mainly compare DeepTheft with the SOTA [28]. For DeepTheft, the sampling rate of energy consumption from the RAPL user interface (i.e., `powercap`) is much lower, i.e., only 1 KHz.

Challenges: To this end, the constraint of *low* sampling rate poses two technical challenges confronted with DeepTheft. The first is to divide energy traces into segments of a target model's layers to accurately recover a complete network

structure and enable subsequent layer-wise hyperparameters inferring. Due to the low sampling rate, we cannot observe salient boundaries among sampling points of different network layers, rendering existing techniques from the SOTA [28] ineffective in addressing this challenge. The second is to infer layer-wise hyperparameters. While some hyperparameters (e.g., kernel size) can be inferred with domain knowledge of model architectures [28], [50], the rest cannot. Particularly, important hyperparameters (i.e., kernel number for a convolutional layer and output feature size in a linear layer) have not yet been addressed by the SOTA, probably because both hyperparameters have a wide range of discrete integer values.

Our Solution: To address the challenges above, DeepTheft designs a novel learning framework that generalizes the extraction of large and deep models (e.g., ResNet152) on advanced hardware. Specifically, DeepTheft hybridizes i) U-Net [35] that is widely used for image segmentation to capture spatial-feature, and ii) BiLSTM (Bidirectional Long Short-Term Memory [28]) to capture temporal-feature. Moreover, the performance of this hybrid model design is ensured by constructively-designed loss functions. With this hybrid design, DeepTheft can recover all layers and divide an unknown energy trace into segments of sampling points that correspond to distinct layer types. Based on the segments of distinct layers, DeepTheft can then infer most layer-wise hyperparameters via common classification tasks. To infer the important hyperparameters of kernel number and output feature size, we note that there exists an inadvertent linear approximation between a segment of a convolutional (linear) layer and the computing overhead of the layer's operations. Further, the computing overhead is correlated with all the layer's hyperparameters including kernel number (output feature size). With this insight, we perform a regression task against the computing overhead of convolutional (linear) layers, and then successfully infer kernel number (output feature size) based on the correlation.

This newly designed learning framework is also applicable to other time-series side channel signals. For validation, DeepTheft exploits another recent revealed side channel, DVFS (dynamic voltage and frequency scaling)-enabled x86 CPU frequency side channel [45]. Compared to the RAPL side channel, this frequency side channel also has a low sampling rate of 1 KHz while it can be accessed unprivileged in the bare-metal OS setting. For the rest of the paper, we *focus on* the RAPL side channel and present our evaluation of the frequency side channel in Section 5.5.

Our contributions/results are summarized as follows¹:

- DeepTheft is an end-to-end attack, that, for the first time, demonstrates that either the power or CPU frequency side-channel can be used to successfully exfiltrate large and deep DNN model architecture information on general processors. In contrast to existing mainstream side-channel based model stealing attacks except [50], DeepTheft requires neither physical proximity nor access to target machines.

1. The source code and large-scale dataset are released at <https://github.com/LearningMaker/DeepTheft>.

- We propose a *new general learning framework* that consists of a set of meta-models as existing work is ineffective in addressing newly raised challenges. Specifically, In the offline phase, the framework learns the correlations between time-series signals (e.g., energy traces) and DNN model architectures. In the online phase (where the stealing attack occurs), the pretrained meta-models surgically segment a time-series signal from an unknown model inference, resulting in an accurate network-structure recovery and timer-series signal segments. Further, the meta-models accurately infer layer-wise hyperparameters. We note that a single power trace per unknown model architecture is sufficient for stealing during the online inference phase.

- We perform a comprehensive evaluation of DeepTheft in an MLaaS setting of the latest docker environment. Particularly, we construct a large training dataset including 50,000 energy traces from 10,000 model architectures of prevalent model families to train the meta-models. In the online phase, the pretrained meta-models are tested against a test dataset of 5,760 energy traces from 1,152 unknown model architectures. The experimental results show that DeepTheft demonstrates a high LDA of 99.75% in recovering network structures, and a high weighted average F1 score of 99.60% in inferring diverse layer-wise hyperparameters, including the kernel number and the output-feature size that have not been addressed by the SOTA [28]. Also, we compare DeepTheft with the SOTA by using their open-source code in the same setting, results of which show that DeepTheft performs much better (41% LDA higher) than the SOTA in recovering the network structure.

- We further validate the generalization of the learning framework by using another time-series side channel signal, i.e., CPU-frequency, in a bare-metal Ubuntu 18.04.6 LTS server. Our evaluation shows that DeepTheft with the CPU-frequency side channel has achieved a high attacker performance in stealing model architectures, similar to that with the power side channel.

Responsible Disclosure. DeepTheft exploits a publicly known power side channel² and a CPU frequency side channel³ and thus there is no need to report it to the CPU vendors. This is similar to DeepSteal (Oakland’22) [32] that exploited a publicly known rowhammer-based side channel⁴ to steal model weights. However, as RAPL is still accessible to docker containers, we have disclosed this security issue to the docker security team on 13th, July, 2023. The team has acknowledged it and set an embargo date until 19th, September, 2023 before releasing its fix.

2. See CVE-2020-8694 and CVE-2020-8695 from <https://platypusattack.com/>.

3. See CVE-2022-23823 (AMD) and CVE-2022-24436 (Intel) from <https://www.hertzbleed.com/>

4. See CVE-2019-0174 from <https://rambleed.com/>.

2. Background

2.1. Deep Neural Network (DNN)

A DNN is composed of multiple layers of interconnected artificial neurons to map the linear or non-linear relationship between input data and output data. A DNN has two stages: training and inference. As the training process is computationally heavy, it is often performed on GPUs. However, attributing to cost-efficiency, CPUs are also used to support the DNN inference for good responsiveness [50] e.g., AWS [3], Google [16] and Alibaba Clouds [1] all supporting CPU inference.

DNN Architecture: As substantial human intelligence and intensive computing resources are often required to develop DNN model architectures, the architecture has become the intellectual property and a primary target for attackers. A DNN architecture is decided by a list of *hyperparameters* including the structure and layer-wise hyperparameters. Aligned with previous model-stealing attacks [28], [46], [50], we aim at stealing the following hyperparameters:

- the number of layers (e.g., ResNet152 has 152 layers);
- the type of each layer (e.g., fully-connected layer, convolutional layer and pooling layer);
- the activation function for each layer (e.g., `relu`);
- the layer-wise hyperparameters for a specific layer, e.g., the neuron number for a fully-connected layer; the kernel size for a convolutional layer, the stride size for a pooling layer.

2.2. RAPL

Intel has introduced the RAPL feature to enable power management since its SandyBridge microarchitecture [27], [55]. Particularly, the Intel RAPL provides energy consumption of underlying hardware to software at a granularity of the so-called *domain*. Intel defines five main domains, that is, *Package* is the entire CPU socket; *Power planes 0 and 1* (PP0 and PP1) refer to the processor cores and uncore devices on the socket, respectively; *DRAM* is the main memory attached to the memory controller; *Platform* covers the whole system-on-chip.

Moreover, multiple model-specific registers (MSRs) are defined to serve the energy estimation and they can be accessed by privileged software (e.g., kernel). To help unprivileged software acquire energy estimates for each domain, Intel has implemented a power capping framework for Linux (i.e., `powercap`) since Linux kernel 3.13, which reads values via relevant MSRs and provides them to user-space access via the interface named `sysfs`. Since the RAPL side-channel has been discovered [27], only root-privilege users have meaningful access to the `sysfs` interface, that is, read access by unprivileged users returns 0 only.

Nevertheless, at the time of writing this paper, we observe that the interface is still accessible to a container in the latest docker version of 20.10.18. Additionally, certain AWS EC2 instances are allowed to access RAPL MSRs.

While DeepTheft is demonstrated on the Intel CPUs, we note that AMD CPUs also introduce the RAPL feature since its Zen microarchitecture and even provide energy estimates at the per-core level, a finer granularity compared to the PPO domain in the Intel CPUs.

3. Related Work

Side-Channel based Model Architecture Stealing: A large number of attacks [7], [10], [23]–[25], [28]–[30], [32], [41], [46]–[51], [54], [56] have been proposed to leverage different side-channel leakage to break data confidentiality relevant to DNN security, among which some representative works and DeepTheft are shown in Table 1. While a few works can extract model parameters such as weights [32]⁵ or recover model inputs [41], [47], most of the them [7], [10], [23]–[25], [28]–[30], [46], [48]–[51], [54], [56] focus on stealing model architectures. Existing model-stealing attacks generally assume no prior knowledge about a target model and rely on different side-channel leakage sources, e.g., power [10], [29], [48], [49], [54], memory-access pattern [24], computer bus [23], [56], electro-magnetic (EM) emanations [7], [25], [28], [51], cache [50], or GPU features (i.e., context switch [46] and performance counters [30]). In the following, we discuss these attacks based on whether they require physical proximity or access to a target machine where a victim model is residing. The DeepTheft does not require such proximity/physical access.

Table 1: DeepTheft and representative works (in chronological order) that use side-channels to compromise data confidentiality of deep learning.

Work	Side Channel	No Physical Proximity/Access?	Targeted Hardware
Hua <i>et al.</i> [24] (DAC'18)	Memory Access Pattern	×	FPGA
CSI NN [7] (USENIX SEC'19)	Electro Magnetic Emanation	×	MCU
DeepSniffer [23] (ASPLOS'20)	Computer Bus	×	GPU
Cache Telepathy [50] (USENIX SEC'20)	Cache	✓	CPU
Hermes Attack [56] (USENIX SEC'21)	Computer Bus	×	GPU
DeepSteal [32] (Oakland'22)	Rowhammer	✓	DRAM
Maia <i>et al.</i> [28] (USENIX SEC'22)	Electro Magnetic Emanation	×	GPU
DeepTheft (Ours)	Power (and CPU Frequency)	✓	CPU

• *With Proximity/Physical Access.* To recover a victim model architecture, one class of side-channel attacks relies on customized equipment for side-channel information collection and requires either physical proximity [7], [10], [25], [28], [48], [49], [51] or physical access [23], [24], [56] to targeted machines. Batina *et al.* [7] leveraged both model querying and EM probing to extract shallow neural networks (no more than 20 layers) running on edge microcontrollers (MCUs). Yu *et al.* [51] also leveraged the EM side channel to recover binarized neural networks that are tailored for edge devices. Chmielewski *et al.* [10] performed a simple EM and power analysis to partially recover targeted MLP and CNN models (e.g., CNN lay-wise hyperparameters are not

5. In [32], an attacker is assumed to know the model architecture of the victim model as prior knowledge.

yet extracted) on an edge device (i.e., Nvidia Jetson Nano). Wolf *et al.* [48] conducted a simple power analysis using a specialized device (i.e., a ChipWhisperer Lite) against an MCU to differentiate one model from another. Xiang *et al.* [49] revealed model architectures via power traces in a raspberry-pi platform. Different from prior works that exploited near-field EM signals, Liang *et al.* [25] collected far-field EM traces via a specialized device, which can be several meters away from a victim machine. Their proposed attack was demonstrated on an NVIDIA GPU to recover shallow model architectures. Hua *et al.* [24] analyzed off-chip memory-access patterns via a hardware trojan insertion and reverse-engineered structure and weights of a shallow model running at an edge FPGA accelerator. Hu *et al.* [23] combined EM traces and bus snooping to generate statistics of memory reads/writes, patterns of which are analyzed to infer complex model architectures on advanced GPU. Different from them, Maia *et al.* [28] could recover layer-wise hyperparameters for extracted layers more precisely by analyzing GPU-emitted magnetic signals via a physical sensor. Similar to [23], Zhu *et al.* [56] developed a bus snooping approach to capture the PCIe traffic between host machines and advanced GPU devices and reconstruct the target model architectures.

• *Without Proximity/Physical Access.* Compared to the aforementioned class of attacks, the other class of side-channel attacks [29], [30], [46], [50], [54] that need co-location between an attacker and a victim in the same physical machine are more applicable to the MLaaS clouds where physical proximity or physical access is almost impossible to an attacker. With an in-depth code analysis of the implementation of Generalized Matrix Multiply, Yan *et al.* [50] leveraged a cache side channel in x86 CPU to infer the architecture of a complex model. Naghibijouybari *et al.* [30] abused the CUDA profiling tools interface of Nvidia GPU as performance counters to sample performance events from a victim DNN model and thus partially infer the model architecture, i.e., the number of neurons of the model’s input layer. To address the limitation, Wei *et al.* [46] exploited the penalty of Nvidia GPU’s context switches. Their proposed attack could slow down the transition between DNN layer operations to collect enough samples per DNN layer operation and improve its accuracy for predicting a shallow model architecture. Zhang *et al.* [54] used a power sensor (e.g., ring oscillators) to collect power traces from a victim model in a shared FPGA platform that supports multi-tenancy. Also in this shared FPGA setting, Meyers *et al.* [29] took network folding into consideration and recovered the folding parameters with power side-channel analysis. We note that the multi-tenancy FPGA platform has not yet been commercialized whereas the current cloud provides only support for single-tenancy FPGA.

Query based Model Stealing: Query based attack mainly attempts to obtain a model that shares similar behavior to the victim model (i.e., prediction between the stolen model and victim model is consistent, namely model fidelity) and cannot steal model architectures [9]. In this attack, the

attacker queries the victim model with (limited) number of samples and gains corresponding outputs (e.g., softmax or single label) provided by the victim model. Those sample-label pairs are then used to train a substitute model that attempts to have comparable fidelity to the victim model. Therefore, the attacker can avoid paying for queries later to the model provider. However, sample query based model stealing [42], [44] is inefficient against complicated models unless the model architecture is known [31].

4. DeepTheft

In this section, we first give our threat model, and then introduce the overview and design details of DeepTheft.

4.1. Threat model

Aligned with previous side-channel based model stealing attacks [7], [28], [32], [50], [51], we assume an attacker aims to steal the architecture (i.e., network structure and layer-wise hyperparameters) of a target DNN model providing the inference service. We further assume the attacker can leverage prior techniques [5], [12], [34], [43], [53] to co-locate herself onto the targeted machine as the victim model, which is practical in a shared-cloud scenario, e.g., the prevalent MLaaS [33]. In our implementation, we use the recent docker environment of version 20.10.18 to simulate a container cloud for a comprehensive evaluation [15]. Particularly, the attacker, residing in a docker container, has legitimate access to the `powercap` interface but is not allowed to access another docker container running the model, as the docker environment in the targeted machine is benign and deploys proper container isolation. All the container images can be different and they are pulled from the official Docker hub. In Section 6, we also demonstrated the potential of using DeepTheft for model stealing in the AWS setting where an attacker residing in an EC2 instance is allowed to extract the energy consumption via RAPL MSRs. Last, DeepTheft is a black-box attack assuming no prior knowledge about the targeted DNN model. The attacker can only feed inputs to the target model through a legitimate query interface [42], passively and non-intrusively collect the energy traces from the shared machine and analyze them for model-architecture stealing. Given an unknown model architecture, a single query or snapshot fed into the unknown running model is sufficient in stealing the model.

4.2. Overview

DeepTheft has two phases, i.e., offline and online, as shown in Figure 1. In its offline phase, DeepTheft develops a constructive learning framework that consists of a set of meta-models. These models are trained upon a dataset, which has a large number of energy traces from large neural networks of various model architecture families (e.g., AlexNet, VGG, ResNet, and random architectures). For each energy trace, the attacker performs sampling for all available

domains via the `powercap` interface to collect sampling points. The sampling can be conducted from a machine model same to the victim machine. After that, each sampling point is labeled with a ground-truth layer type (e.g., linear layer, convolutional layer and pooling layer).

In its online phase, DeepTheft queries a black-box target model in the victim machine to trigger its model inference and capture its energy trace. With the energy trace, DeepTheft implements a two-step attack. In the first-step, a pre-trained meta-model gained in the offline phase, coined *MetaModel_{Stru}*, is used to perform a surgical segmentation against the energy trace, resulting in segmented points corresponding to different layers of an accurate network structure (e.g., the number of layers and the layer type). In the second step, with the segmented points of each layer, DeepTheft leverages multiple other pretrained meta-models (called *MetaModels_{Hyper}*) and domain knowledge to infer layer-wise hyperparameters.

Clearly, the performance of the meta-model training in the offline phase is critical to the effectiveness of the model architecture stealing in the online phase. In the online phase, the accuracy of *MetaModel_{Stru}* affects the accuracy of *MetaModels_{Hyper}*, as inferring the layer-wise hyperparameters is dependent on the trace segmentation that segments the trace into layers precisely—all points corresponding to a layer are fed into *MetaModels_{Hyper}* for layer-wise hyperparameters inferring. To this end, the challenges of DeepTheft are to acquire a well-trained *MetaModel_{Stru}* and *MetaModels_{Hyper}*.

Specifically, the first challenge is to train *MetaModel_{Stru}* so that it can divide an unknown energy trace into segments of sampling points (each segment predicted with a layer type), and enable subsequent layer-wise hyperparameters inferring for *MetaModels_{Hyper}*. For this challenge, an intuitive solution is to leverage Bidirectional Long Short-Term Memory (BiLSTM) [19] from the SOTA [28] for capturing the temporal features (e.g., the chronological sequence of the sampling points) of a given energy trace. However, the SOTA has a high sampling rate (no less than 47 KHz) and thus can observe the salient boundaries among the sampling points caused by the execution of different layers. For *MetaModel_{Stru}*, applying BiLSTM would result in points mis-segmentation, that is, some points will be mis-classified into a wrong layer type (we compared *MetaModel_{Stru}* with BiLSTM in the SOTA in Section 5.4), as DeepTheft has a sampling rate of only 1 KHz. To address this challenge, *MetaModel_{Stru}* is inspired by U-Net [35], a popular model architecture for extracting spatial features of 2D (Dimensional) images. In *MetaModel_{Stru}*, the U-Net is used to extract the spatial features of the 1D energy traces, e.g., the sampling points in a trace can exhibit distinct visual shapes. However, the U-Net itself is ineffective to capture temporal features provided by the time-series energy trace and missing the rich temporal information per se. *MetaModel_{Stru}* addresses this by incorporating BiLSTM to capture both spatial features with the U-Net, which form a new hybrid architecture. Further, a new loss function is carefully

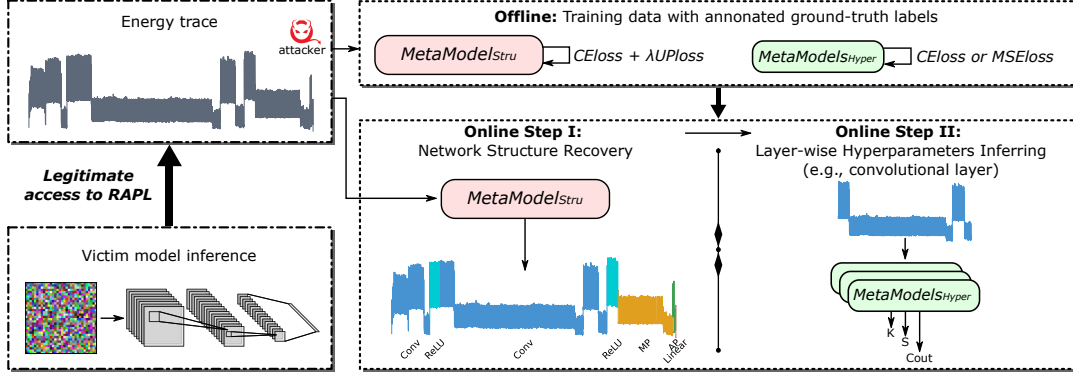


Figure 1: An overview of DeepTheft.

designed for $MetaModel_{Stru}$ to learn correlations among sampling points from within-one-layer to across-layers.

The second challenge is to train $MetaModels_{Hyper}$ so that it can infer layer-wise hyperparameters for a given segment of sampling points (each segment is marked by $MetaModel_{Stru}$ with a layer type). While some hyperparameters can be decided using domain knowledge (e.g., the input kernel number is equal to the output kernel number of a convolutional layer), there are 7 hyperparameters (see Table 2) that need to be inferred using $MetaModels_{Hyper}$. Among them, 5 hyperparameters (e.g., kernel size in a convolutional layer) have a much small range of value candidates and thus $MetaModels_{Hyper}$ can infer them via common classification tasks. The challenge is to infer the kernel number in a convolutional layer and the output feature size in a linear layer, as both have a wide range of discrete integer values. (e.g., 2^n where n can be from $\{4, 5, 6, \dots\}$) and they can hardly be covered by the energy traces. Thus, it is hard to infer them via a classification task. It is also inaccurate to perform regression tasks against them as there is no direct correlation between the energy traces and either of them. This might be the reason why the SOTA [28] did not infer them. To address this challenge, we observe that for a segment of sampling points for a specific layer-type, it has linear approximation with the computing overhead of the layer’s operations, which are correlated by all the layer’s hyperparameters. Thus, either the kernel number or the output feature size is one of the hyperparameters that correlate linearly with the computing overhead. With this observation, we perform an indirect regression against the computing overhead of convolutional/linear layers, and then indirectly infer the hyperparameter (kernel number/output feature size) based on its correlation with the overhead. To this end, we customize $MetaModel_{Stru}$ to generate $MetaModels_{Hyper}$ ’s model architectures for either classification tasks or indirect regression tasks.

In the following, we discuss the design of $MetaModel_{Stru}$ in Section 4.3, domain knowledge in Section 4.4 and $MetaModels_{Hyper}$ in Section 4.5.

4.3. $MetaModel_{Stru}$ Design

We first introduce the model architecture of $MetaModel_{Stru}$, and then discuss how to formulate its loss function for effective learning.

4.3.1. Model Architecture. As shown in Figure 2, the backbone network of $MetaModel_{Stru}$ is a hybrid design of U-Net and BiLSTM, which extracts spatial features and temporal features from an input time-series energy trace, and outputs a segmentation map, which is a matrix of predicted probabilities of layer types for all sampling points in the trace.

Capturing Spatial Features via U-Net: U-Net is made up of a set of 1D CNNs, which consists of a down-sampling path (contracting path) on the left of Figure 2, and an up-sampling path (expanding path) on the right of the figure. The down-sampling path has four encoders, which down-sample a spatial feature map step-by-step using the maxpooling operation and thus gradually aggregate the spatial information into semantic information. In this process, the spatial feature map is eventually abstracted into a rich-semantics feature map. The up-sampling path has four symmetric decoders, which up-sample the abstracted feature map step-by-step using linear interpolation and thus gradually restore the spatial information with the semantic information preserved.

Both the encoders and decoders are based on residual blocks to mitigate the gradient vanish issue [22]. To compensate for the information lost from the down-sampling path, a feature map output by each encoder is fused via a channel (i.e., a skip-connection operator denoted as a dashed line with an arrow in Figure 2) into a decoder along the up-sampling path. By fusing the low-level features with high-level features, the decoders can restore the encoders’ abstracted information from the time-series trace, thus improving $MetaModel_{Stru}$ ’s performance.

Capturing Temporal Features via BiLSTM:

At the bottom of Figure 2, a BiLSTM-based temporal encoder is placed, which takes the spatial feature map from the last encoder of U-Net as input and enhances the learning of temporal features. As the input of the temporal encoder is the smallest spatial feature map (downsampled by 16 times)

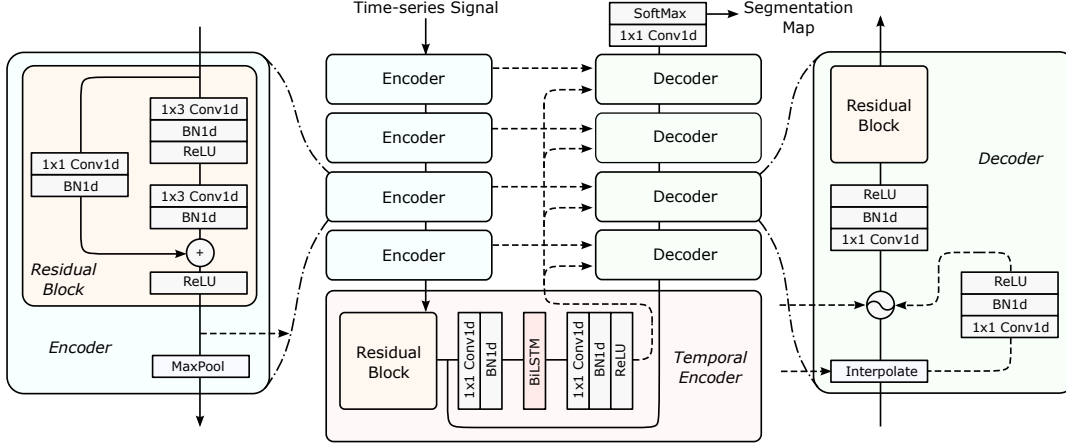


Figure 2: The model architecture of $MetaModel_{stru}$. Its input is a time-series signal (e.g., an energy trace of sampling points for DeepTheft). Its output is a segmentation map, which is a matrix of predicted probabilities of layer types for all sampling points in the trace.

from U-Net, it improves the BiLSTM’s training efficiency. Besides, its high-level semantics facilitate the capture of temporal features. Thus, the output of the temporal encoder is rich in temporal features. To better combine temporal features and spatial features, the temporal encoder provides an additional channel (a skip-connection operator) as an input to each decoder.

As the input to $MetaModel_{stru}$ is an energy trace from a model inference, its length can be varied. Thus, we pad the input with a factor of 16, given that the 4 encoders downsample the energy trace by a factor of 16. We note that $MetaModel_{stru}$ is designed to generalize the time-series energy trace segmentation and thus it is also applicable to other time-series signals, such as the EM signals from the SOTA [28].

4.3.2. Loss Function in Training. Suppose we have obtained a dataset consisting of N energy traces $\mathcal{D} = \{\mathbf{x}^i, \mathbf{y}^i, \mathbf{z}^i\}_{i=1}^N$ (the dataset construction is deferred to Section 5.1). Here, each $\mathbf{x}^i \in \mathbb{R}^{c \times l}$ is an energy trace of performing a model inference. Each trace has c channels corresponding to the RAPL’s domains (e.g., DRAM) and l samples (e.g., one sampling point every 1ms in our dataset as the sampling rate is 1 KHz), with each sample \mathbf{x}_s^i having a layer type \mathbf{y}_s^i , a k -dim one-hot encoding vector for k layer types (e.g., pooling layer, convolutional layer, ReLU). Thus, the aforementioned segmentation map is a $l \times k$ matrix. $\mathbf{z}^i \in \mathbb{N}^{n \times 2}$ is the position label matrix for n layers in the energy trace \mathbf{x}^i , where each row records the start and end position of the respective layer. We note that \mathbf{z}^i is only required during the offline phase to train the meta-models and will not be used in the online phase. With this dataset, we discuss how to design our loss function for $MetaModel_{stru}$.

Specifically, the model is denoted as f with parameters θ , and $f_\theta(\mathbf{x}^i) \in \mathbb{R}^{k \times l}$ is to map an energy trace $\mathbf{x}^i \in \mathbb{R}^{c \times l}$ to its confidence scores, where $f_\theta(\mathbf{x}^i)_s$ indicates the probability vector of predicting a sample point s in \mathbf{x}^i .

Sampling-Point-Independent Loss: A possible way to

train $MetaModel_{stru}$ is by minimizing the standard cross-entropy (CE) loss as below:

$$\mathcal{L}_{CE} = - \sum_{\mathbf{x}^i, \mathbf{y}^i \in \mathcal{D}} \sum_s^l \mathbf{y}_s^i \log(f_\theta(\mathbf{x}^i)_s). \quad (1)$$

However, training the model with the CE loss alone cannot achieve high accuracy for two main reasons. First, the CE loss is the sum of the losses of all sampling points with the same weight (i.e., 1) and the number of points corresponding to different layers can be highly imbalanced. Take an energy trace we collected as an example, one convolutional layer occupies more than half of the points, while a linear layer has as few as 1 or 2 points. Thus, the CE loss is not effective in handling imbalanced sampling points, as minimizing it would mislead the model to predict all sampling points into the layer types with more points, making the layer type with few points ignored. Second, considering that the CE loss predicts a layer type per sampling point, it cannot capture the contextual information among neighbors of a point and thus cannot ensure that the predicted layer types for the neighbors are consistent.

Cross-Sampling-Point Loss:

To address the aforementioned problem, we propose a complementary loss, termed Unique Path (UP) Loss, which is inspired by CTC Loss [18], a solution mainly used to segment non-sequential data. Compared to the CTC Loss, the UP loss has a different design for two considerations. First, the CTC Loss allows identical layer prediction in its prediction sequence, which does not hold for $MetaModel_{stru}$ as a model does not have consecutive identical layers. Second, as inputs are unnecessarily aligned with outputs, the CTC Loss needs to find all possible paths to make a correct prediction, which incurs a high computational overhead. For $MetaModel_{stru}$, its inputs and outputs are inherently aligned, and thus the UP loss only needs to identify the unique possible path for a correct prediction, which is much more efficient.

Specifically, we first apply each position label \mathbf{z}_m^i to isolate the sampling points in \mathbf{x}^i corresponding to a layer.

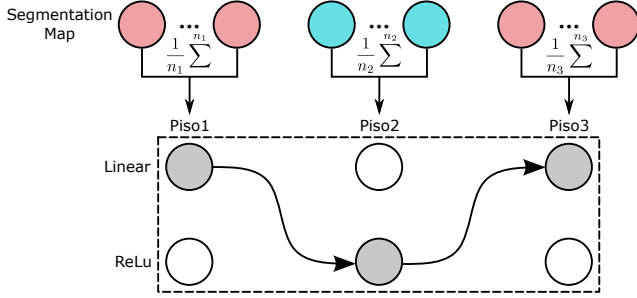


Figure 3: An illustrative example of using UPL in an MLP with three layers [Linear, ReLu, Linear]. It first averages the probabilities of the successive classes in the segmented map and aggregates them to the probabilities (P_{iso}) of the isolated sampling points, and then multiplies P_{iso} to all layers to obtain the unique path probability.

Then we compute the unique path probability for this layer, which is defined as the average prediction probability of the isolated sampling points in this layer as:

$$P_{iso}(\mathbf{z}_m^i) = \frac{\sum_{s=z_{m,0}^i}^{z_{m,1}^i} \mathbf{y}_s^i f_{\theta}(\mathbf{x}_s^i)}{z_{m,1}^i - z_{m,0}^i + 1}. \quad (2)$$

In principle, the layer corresponding to $P_{iso}(\mathbf{z}_m^i)$ is deterministic in a one-to-one manner, and $P_{iso}(\mathbf{z}_m^i)$ can represent the probability of all sampling points within \mathbf{z}_m^i being predicted correctly. Then, we multiply $P_{iso}(\mathbf{z}_m^i)$ for all layers in the energy trace to represent the unique path probability for all layers as shown in Figure 3, which can measure the closeness between all the predicted layers and the ground-truth layers. Formally, the UPL is defined as follows:

$$\mathcal{L}_{UP} = - \sum_{\mathbf{z}^i \in \mathcal{D}} \log\left(\prod_{m=1}^n P_{iso}(\mathbf{z}_m^i)\right). \quad (3)$$

The UPL captures the relationships among neighboring points and minimizing it encourages consistent prediction of sampling points from the same layer. As the UPL is defined on layers instead of sampling points, it can also alleviate the issue of imbalanced sampling points of different layers.

Loss Function Formulation for $MetaModel_{Stru}$: The ultimate loss used to train the $MetaModel_{Stru}$ is formulated as below:

$$\mathcal{L} = \mathcal{L}_{CE} + \lambda \mathcal{L}_{UP}, \quad (4)$$

where λ is a hyperparameter to balance the two losses (e.g., $\lambda = 1$ by default). To this end, \mathcal{L}_{CE} aims to achieve an accurate prediction per sampling point, and \mathcal{L}_{UP} is carefully designed to learn the context information of sampling points from within a layer (i.e., isolating points from a layer via \mathbf{z}_m^i) and different layers (i.e., maximizing the unique path probability for all layers). Hence, the UP loss can capture both spatial and temporal features.

Table 2: A list of layer-wise hyperparameters for the three layers. If those marked in red are inferred via $MetaModels_{Hyper}$, the rest can then be decided (Hypers, Conv and MP denote Hyperparameter, Convolutional, and Max Pooling, respectively).

Layer	Hypers	Description
Conv	C_{in}	Number of channels of an input. Its value is decided by the input or C_{out} .
	C_{out}	Number of kernels. Its value is 2^n where n can be from $\{4, 5, 6, \dots\}$.
	K	Size of a kernel. Its value is from $\{1, 3, 5, 7\}$.
	S	Stride. Its values is from $\{1, 2\}$.
	P	Size of padding. Its value is decided by $\lfloor (K-1)/2 \rfloor \times D$.
	D	Dilation. Its value is set to 1.
	G	Groups. Its value is set to 1.
MP	K	Size of a kernel. Its value is from $\{2, 3\}$.
	S	Stride. Its value is from $\{1, 2\}$.
	P	Size of padding. Its value is from $\{0, 1\}$.
	D	Dilation. Its value is set to 1.
Linear	F_{in}	Size of input. Its value is decided by F_{out} or C_{out} .
	F_{out}	the size of output. Its value is decided by the number of classes or 2^n where n can be from $\{4, 5, 6, \dots\}$.

4.4. Domain Knowledge

Aligned with the SOTA [28], popular and complex network families (e.g., MLP, AlexNet, VGG and ResNet) are composed of three layer types: convolutional layer, maxpooling layer; and linear layer. Each type of layer has different layer-wise hyperparameters. We summarize them in Table 2, Note most of these hyperparameters are correlated, so that can be deterministically derived upon domain knowledge. The domain knowledge of each hyperparameter is summarized in Table 2 and detailed in Section A in Appendix.

Based on domain knowledge, $MetaModels_{Hyper}$ needs to infer three hyperparameters (i.e., C_{out} , K , and S) for the convolutional layer, three hyperparameters (i.e., K , S , and P) for the maxpooling layer and one hyperparameter (i.e., F_{out}) for the linear layer. When these hyperparameters are inferred by $MetaModels_{Hyper}$, other hyperparameters can be deterministically derived from them. As each of these 7 hyperparameters has its own characteristics, $MetaModels_{Hyper}$ consists of 7 distinct meta-models, which are introduced in the following section.

4.5. $MetaModels_{Hyper}$ Design

For each meta-model of $MetaModels_{Hyper}$, we customize the architecture of $MetaModel_{Stru}$ by retaining the 4 encoders but adding a fully connected layer for either classification or regression (on whether the hyperparameter inferring is a classification or a regression task).

As C_{out} and F_{out} have a large range of discrete values, it is almost impossible to collect the energy traces that can cover all their possible values, making it hard to infer them via classification tasks. An intuitive solution is to use regression tasks with a standard loss function, i.e., mean-square-error (MSE). However, a direct regression against either C_{out} or F_{out} is inaccurate as either one has no direct relationship with segments of sampling points predicted to

their respective layer type. We discuss how to address this challenge with a key observation later.

For other 5 hyperparameters, they have a much smaller range of value candidates and thus can be inferred via classification tasks with a standard cross-entropy (CE) loss function. During the training, the objective is to minimize the CE loss of ground-truth hyperparameter values and the estimated ones. We note that when training each meta-model of $MetaModels_{Hyper}$ in the offline phase, the inputs to a model are segmented sampling points of a specific ground-truth layer type. In the online phase, the inputs to each model are a segment of sampling points predicted by $MetaModel_{Stru}$ to a layer type.

Model Training for Indirect Regression Tasks:

To infer C_{out} , we observe that for a convolutional-layer segment of sampling points, it has linear approximation with the computing overhead of a convolutional layer operations (denoted as O_c). Further, O_c is decided as follows:

$$O_c = (C_{in} \times K \times K) \times (C_{out} \times H_{out} \times W_{out}) \times bs. \quad (5)$$

In this definition, the first bracket represents the computing overhead of a convolutional kernel that only needs to be computed once. The second bracket indicates the number of operations of the convolutional kernel. bs is for batch size. H_{out} and W_{out} respectively denote the height and width of an output feature map, which can be determined by the hyperparameters of a convolution layer as well as the height H_{in} and width W_{in} of an input feature map. We note that H_{in} and W_{in} are similar to C_{in} as they can be known if a preceding layer’s hyperparameters are decided. For H_{out} and W_{out} , they need to satisfy the following two equations:

$$H_{out} = \lfloor (H_{in} + 2 \times P - D \times (K - 1) - 1) / S \rfloor + 1. \quad (6)$$

$$W_{out} = \lfloor (W_{in} + 2 \times P - D \times (K - 1) - 1) / S \rfloor + 1. \quad (7)$$

In these equations, K and S are inferred by corresponding meta-models, thus making P be derived by aforementioned domain knowledge (i.e., $P = \lfloor (K - 1) / 2 \rfloor \times D$). Thus, H_{out} and W_{out} can be decided.

Further, all the parameters on the right side of Equation 5 can be decided except C_{out} , and we can see that O_c is linear to C_{out} , indicating that the regression task against C_{out} can be transferred to the regression against O_c . Specifically, we first logarithmize O_c to prevent numerical overflow, and then perform a regression task against $\log(O_c)$ via minimizing the MSE between the ground-truth computing overhead and the estimated one. We then decide C_{out} based on Equation 5. Based on the aforementioned description of C_{out} in Section 4.4, C_{out} is inferred by rounding its regressed value to a nearest value in the form of 2^n , i.e., $2^{\text{Round}(\log_2 C_{out})}$.

For F_{out} in the linear layer, we can similarly adopt the transferred solution of inferring C_{out} to infer F_{out} . Specifically, we define the computing overhead of a linear layer’s operations (denoted as O_f) as $O_f = F_{in} \times F_{out} \times bs$. With this observation, we perform a direct regression against O_f , and then infer F_{out} as F_{in} and bs are known.

5. Evaluation

In the online phase of DeepTheft, the target machine where a victim model is running has Intel Xeon W 2123 (8 logical cores) and 16 GB DRAM. The DeepTheft attack and victim model inference run in two separate containers, managed by the underlying container scheduler. The attacker has no knowledge of the core where the victim model inference is running. Its system software is Ubuntu Server 18.04.6 LTS (kernel version 4.15.0-193-generic) with the latest Docker version 20.10.18 installed, where an attacker residing in one container can collect the energy traces via the `powercap` interface when the victim model from another container starts to perform the inference. Both containers’ images are pulled from the docker hub (i.e., Ubuntu 22.04.1 LTS) and they can be different. The victim model uses PyTorch 1.10.1 with Python version 3.6.9 as its underlying deep learning framework. Without loss of generality, this machine is also used in the offline phase to collect the energy traces as the dataset for meta-models training.

All meta-models are trained in a machine with an NVIDIA GeForce RTX 3070 GPU (8 GB video memory), Intel i7-11800H CPU (16 logical cores) and 16 GB DRAM memory. The deep learning framework used here is PyTorch 1.10.1 with Python version 3.8.10.

In what follows, we first describe how to construct a large-scale training/test dataset for $MetaModel_{Stru}$ and $MetaModels_{Hyper}$ in Section 5.1. We then use the dataset to train and test $MetaModel_{Stru}$ and $MetaModels_{Hyper}$ in Section 5.2 and Section 5.3, respectively. We note that the test dataset is used to simulate the online phase of DeepTheft so as to evaluate the attack performance of each meta-model.

5.1. Training/Testing Dataset Construction

Sampling Energy Consumption from the RAPL: As the RAPL provides an energy meter via the `powercap` interface, it is accessed to sample the energy consumption for the period of a complete model inference, which is triggered by feeding a batch of images. We note that the energy consumption from two RAPL domains are collected, i.e., PPO and DRAM, corresponding to two channels of energy traces for our dataset. To ease the energy trace collection, `time.sleep(1)` is used to sleep for 1 second before and after the model inference. We note that `time.sleep(1)` is removed during the online phase of DeepTheft, because the attacker can trigger a victim DNN model to start inference by feeding an input and the energy trace of the model inference is distinguishable from that when the model inference is not running.

Annotating An Energy Trace: $MetaModel_{Stru}$ and $MetaModels_{Hyper}$ are trained in a supervised way, thus requiring energy-trace annotation. Particularly, every sampling point in a collected energy trace is required to be annotated with a ground-truth layer-type label. For a segment of sampling points that is labeled with a specific layer type, they are annotated with corresponding hyperparameters’ values. As a large number of energy traces will

Table 3: A constructed dataset for training and testing. For each model architecture, 5 different energy traces under 5 different input sizes are collected. (the number of model architectures; the number of energy traces).

Dataset	Total	VGG	ResNet	RandomNet
Training	(10,000; 50,000)	(460; 2,300)	(4,648; 23,240)	(4,892; 24,460)
Test	(1,152; 5,760)	(52; 260)	(536; 2,680)	(564; 2,820)

be collected from the model inference of different model architectures, manually annotating these energy traces is extremely tedious and costly. To address this issue, popular deep learning frameworks do provide profiling interfaces, e.g., `torch.autograd.profiler` in PyTorch and `tf.profiler` in TensorFlow). In our implementation, the PyTorch-provided interface is embedded into a DNN model’s deployment to automate the annotation. We note that DeepTheft in the online phase *does not* need these interfaces.

Constructing Training/Testing Dataset: Aligned with the SOTA [28], the energy traces we collect for the training/testing dataset construction are from a number of model architectures. Specifically, we generate model architectures from two sources. The first refers to popular and widely used model families: AlexNet, VGG, ResNet and their variants are picked here. The variant models are built by randomly changing (i.e., adding or removing) network layers of different layer types, following the design rules of their respective model families. The second is to generate random models, which consist of MLPs with random combinations of only fully connected layers, and convolutional neural networks with random combinations of convolutional layers, activation layers, pooling layers, and possibly normalization layers.

To this end, 11,152 models with different architectures have been acquired, among which there are 512 VGG-family models, 5,184 ResNet-family models, and 5,456 randomly generated models including the structures of AlexNet family models, shown in Table 3. We note that the model number is much larger than that of the SOTA [28], which only considers 564 models (i.e., 500/64 for training/testing). In our generated models, their network depth ranges from the shallowest 2 layers (i.e., 1 convolutional layer and 1 fully connected layer) to the deepest 152 layers (i.e., ResNet152). For the SOTA, its deepest ResNet101 has 101 layers.

Following [22], [36], [39], [40], we consider 5 commonly used input sizes for each model, i.e., $\{331 \times 331, 299 \times 299, 224 \times 224, 192 \times 192, 160 \times 160\}$, and each one with three channels (i.e., an RGB image). The batch size is selected from $\{64, 96, 128, 192, 256\}$ ⁶. In total, 55,760 energy traces are collected for the 11,152 different models (each of the five input sizes is applied to a same model), resulting in 20.4 GB. Considering the proportion of the models in each of the three model families, 5,760 energy

6. The batch size is constrained by 16 GB memory of our experimental machine. When the input size is increasing, we decrease the maximum batch size to not exceed the memory capacity.

Table 4: The performance of $MetaModel_{Stru}$ in recovering network structures in the first-step of DeepTheft.

Layer	Conv	BN	ReLu	MP (Max. Pool.)	AP (Ave. Pool.)	Linear	Add*	Overall
SA (%)	99.44	97.99	98.02	99.57	92.93	94.43	95.70	99.26
LDA (%)	99.85	99.74	99.76	99.69	99.06	98.47	99.64	99.75

*Add is a vector addition operation in residual shortcut concatenation.

traces are randomly chosen as the test dataset, and the rest are used as the training dataset.

5.2. Network Structure Recovery

To evaluate the structure recovering performance of $MetaModel_{Stru}$, we use two metrics, i.e., Levenshtein Distance Accuracy (LDA) and Segment Accuracy (SA), following the SOTA work [28].

- LDA is the similarity between a predicted structure and a ground-truth structure⁷.
- SA is the percentage of sampling points that are correctly predicted into their ground-truth layer types.

For a model stealing attack, LDA indicates its prediction accuracy of a network structure. It is 100% when a predicated structure exactly matches a ground-truth one. SA measures the segmentation performance of $MetaModel_{Stru}$. Clearly, a higher SA, better performance of $MetaModels_{Hyper}$.

We use the SGD optimizer to train $MetaModel_{Stru}$ at a learning rate of 0.01 in conjunction with a cosine annealing learning rate. The epochs are 100 with a batch size of 32. Before each batch is fed into the model, energy traces in the batch are padded to the length of the longest energy trace in the batch so that the energy traces within the batch are of equal length. This padding operation is equivalent to a potential data enhancement, similar to a random crop in an image.

The performance in terms of LDA and SA of $MetaModel_{Stru}$ on the testing dataset is shown in Table 4. Specifically, LDA for all the layer types are more than 98%. For SA, DeepTheft performs better in recovering layers that require intensive computation (i.e., convolutional layer) than those layers with less intensive computation (e.g., Average Pooling and Linear). This is because the layers with less intensive computation correspond to a smaller number of sampling points. Despite this, SA of all layer types is still greater than 92%. Overall, $MetaModel_{Stru}$ has achieved 99.26% for SA and 99.75% for LDA, respectively. Additionally, we plot the distribution of normalized Levenshtein distances for all the testing energy traces in Figure 7. We see that almost all of them have 0 normalized Levenshtein distances, indicating that the estimated network structures have exactly matched the ground-truth ones.

7. Generally, LDA is a metric related to Normalised Levenstein Distance (NLD) [18], [23], [28]. The Levenstein Distance is a measure of the minimum number of edits required to transform one sequence into another. The allowed edits include insertions, deletions, and substitutions. Thus, LDA is equal to $\{1 - NLD\}$ where NLD shows the error rate.

5.3. Layer-Wise Hyperparameter Inferring

A segment of sampling points for a predicated layer is fed to a corresponding meta-model of $MetaModels_{Hyper}$ to infer the layer-wise hyperparameter value. The configuration (e.g., SGD optimizer, learning rate) of training $MetaModels_{Hyper}$ is the same as $MetaModel_{Stru}$. Before each segment of sampling points as an input is fed into a meta-model, it is normalized and then uniformly resized to a specified length of 1024 sampling points, which is the average length of all the segments of sampling points.

We then try to evaluate the performance of each meta-model in $MetaModels_{Hyper}$ using three metrics, i.e., prediction, recall, and F1 score. Table 5 shows these metrics for the inferred hyperparameters of different layer types. Clearly, all the hyperparameters in the table are accurately inferred, i.e., all the scores in each metric are almost 100%, which is largely attributed to the precise segmentation of $MetaModel_{Stru}$. For the challenges of inferring C_{out} and F_{out} , their scores reach about 99%, which have validated our proposed indirect regression (see Section 4.5). Further, we compare the inferring performance of C_{out} using our indirect regression with that of an intuitive direct regression in Section 6, results of which show our approach performs much better than the direct one.

5.4. Comparing DeepTheft with the SOTA

Despite the SOTA attack [28] is inapplicable to the MLaaS setting, we compare DeepTheft with it for two main reasons. First, both works are based on a learning-based framework to steal model architectures. Second, different from other existing works [46], [50], both have evaluated a large number of large and deep networks, which are prevalent in the real-world.

Qualitative Comparison: While the SOTA [28] has open-sourced its code⁸, its training/test dataset of EM/magnetic signals is not publicly available. Hence, we make a qualitative comparison based on the reported results in [28]. While DeepTheft has a much lower sampling rate than [28] (i.e., 1 KHz vs 47 KHz), it has overall 99.26% SA and 99.75% LDA for the network structure (i.e., network topology in [28]), which are clearly better than the SOTA’s overall 96.8% SA and 88.2% LDA.

For the performance of inferring convolutional layer-wise hyperparameters, the SOTA has tested 1,804 convolutional layers and the accuracy of the layer-wise hyperparameters is between 96%-97% in Table S2 of [28]. Additionally, the SOTA has not shown the accuracy of inferring the kernel number for a convolutional layer, a challenge that has been addressed by DeepTheft. Compared to it, DeepTheft has tested 226,235 convolutional layers and achieved an accuracy of more than 98% (shown in Table 5), including the performance of inferring the kernel number. We note that the SOTA did not provide the statistics of inferring hyperparameters of other layer types (i.e., max pooling

8. The source code of [28] is available at <https://github.com/henriquetmaia/gpuNetSnooper>.

Table 5: Inferring performance of each hyperparameter in the second-step of DeepTheft.

Layer	Hyperparameter	Precision(%)	Recall(%)	F1(%)
Convolutional	C_{out}	98.89	98.98	98.93
	K	99.86	99.98	99.92
	S	99.87	99.77	99.82
MaxPooling	K	100	100	100
	S	100	100	100
	P	100	100	100
Linear	F_{out}	99.18	99.04	99.10
Weighted average		99.58	99.61	99.60

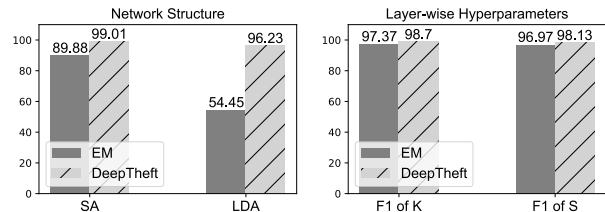


Figure 4: A comparison between DeepTheft and EM (The EM refers to the SOTA attack [28]).

layer and linear layer), which thus we cannot compare with DeepTheft.

Quantitative Comparison: Considering that the first-step is critical to the second-step in both works, we further make a quantitative comparison between them. Specifically, for the first-step, we rely on the SOTA’s open-source code to reproduce its proposed BiLSTM model for segmenting our energy traces. For the second-step, both works use the set of meta-models, i.e., $MetaModels_{Hyper}$. For the training dataset, the SOTA [28] uses 500 models only. Thus, we use the same model number by randomly picking 500 from the 10,000 models in our training dataset. To evaluate the attack performance of the SOTA and DeepTheft, our testing dataset consisting of 1,152 architectures is applied.

The evaluation results are shown in Figure 4. For network structure recovery, the SOTA has only 54.45% LDA, and DeepTheft achieves a much higher LDA of 96.23%, indicating that $MetaModel_{Stru}$ has retained its performance even when the size of the training dataset has decreased significantly from 10,000 to 500. For layer-wise hyperparameters inferring, DeepTheft is slightly better than EM. We note that for both works, only those sampling points that are predicted into correct layer types in the first-step are fed into the second step where our proposed $MetaModels_{Hyper}$ is in use. Thus, while the SOTA shows 89.88% SA, lower than DeepTheft that has 99.01% SA in the first step, the SOTA assisted by $MetaModels_{Hyper}$ in the second step performs much better, i.e., showing higher performance and getting closer to DeepTheft. This demonstrates the efficacy of $MetaModels_{Hyper}$ in inferring layer-wise hyperparameters, and also implies that $MetaModels_{Hyper}$ can tolerate a relatively low SA to an extent.

Training Overhead: As BiLSTM in the SOTA processes the sampling points in a serial way, its execution latency grows linearly with the length of time-series sampling

points. Thus, it is time-consuming for BiLSTM to perform training and inference against a long sequence of sampling points. In comparison, DeepTheft leverages CNN, which processes all the sampling points per energy trace in a concurrent way, resulting in significantly less execution latency. We evaluate the training overhead of BiLSTM and $MetaModel_{Stru}$ using the aforementioned small training dataset of 500 random models, results of which show that $MetaModel_{Stru}$ takes only half a minute per epoch, much less than BiLSTM which requires about 13 minutes per epoch.

5.5. DeepTheft Generalization

DeepTheft can be generic to steal model architecture through other side channels that generate time-series signals. Specifically, we validate that a CPU-frequency side channel [45], also for the first time, can be utilized to accurately steal a target model architecture via our proposed learning framework. For the side channel, it exists in modern x86 processors, where either local or remote attackers could observe DVFS-induced frequency variations depend on the current data being processed, and thus break the data confidentiality of cryptographic software.

In the aforementioned test machine, the same Ubuntu server is running as a bare-metal OS. Within this server, we initiate two unprivileged processes running DeepTheft and a model inference, respectively. Similar to the dataset construction in Section 5.1, DeepTheft leverages an open-source toolkit⁹ to collect CPU-frequency traces at a sampling rate of 1 KHz, which costs two weeks and generates a data volume of 6.8 GB. The data volume consists of 55,760 frequency traces, among which 50,000 and 5760 are used as the training and testing dataset, respectively. Similarly, the traces are from forward inference of the 11,152 different model architectures with the five different input sizes.

While the CPU frequency trace looks significantly different from that of the power side channel (a CPU-frequency trace example is shown in Figure 6 of Appendix), our experimental results of DeepTheft with CPU-frequency traces shows LDA and SA of 99.04% and 99.20%, which are similar to that of using DeepTheft with power traces.

6. Discussion

We first evaluate the impacts of input size and RAPL domains on DeepTheft. We then perform extensive ablation studies on the learning framework. Moreover, we evaluate the impact of noisy workloads on the DeepTheft performance. We further discuss the threat of DeepTheft to commercial clouds. Last, some countermeasures are discussed.

Input Size Impact on DeepTheft: In the above experiments, 5 commonly input sizes are used for models in the training/test dataset. To evaluate the impact of a specified input size on the attack performance of DeepTheft, we also

show the accuracy of recovering network structure and layer-wise hyperparameters for each of the 5 aforementioned input sizes. As shown in Table 6, both overall LDA (indicating the accuracy of network structure recovery) and F1 (showing the accuracy of inferring layer-wise hyperparameters) are similar to each other in different input sizes, indicating that DeepTheft is insensitive to the input size.

Table 6: DeepTheft’s performance is insensitive to the input sizes (batch size, height, width, channel number).

Input Size	Overall LDA(%)	Ave. F1(%)
(256, 160, 160, 3)	99.65	99.63
(192, 192, 192, 3)	99.72	99.59
(128, 224, 224, 3)	99.81	99.58
(96, 299, 299, 3)	99.73	99.62
(64, 331, 331, 3)	99.85	99.61

RAPL Domains Impact on DeepTheft: In the above experiments, both PP0 and DRAM domains provided by the RAPL are used. Here, we compare the attack performance of DeepTheft using both domains with that of using an individual domain. As shown in Table 7, using a single domain can achieve a high recovering accuracy, which can be attributed to our proposed meta-models. Compared to each domain used, using both has slightly better accuracy.

Table 7: DeepTheft’s performance is slightly better when both RAPL domains are used.

RAPL Domain	Overall LDA(%)	Ave. F1(%)
PP0	98.07	98.72
DRAM	97.79	98.88
PP0 + DRAM	99.75	99.60

Direct Regression Against Kernel Number: As discussed in Section 4.5, performing a direct regression task against the kernel number (C_{out}) is not accurate and instead we have proposed an indirect regression approach. Here, Table 8 shows the performance of inferring C_{out} between direct regression and our proposed indirect regression. Clearly, the indirect regression is better in the three evaluated metrics than the direct regression in the default training-dataset size of 50,000. We also reduce the size of the training dataset by 20 times to show its impact on the two methods. For the direct regression, it experiences an obvious performance drop in the decreased size of 2,500 energy traces, which is unacceptable for inferring C_{out} . For the indirect regression, its performance is almost not affected by the decreased size, showing its robustness in inferring C_{out} .

Ablation Study: We perform an ablation study of our proposed learning framework. Particularly, to show its attacking effectiveness, we remove its critical components and losses. As mentioned in Section 5.4, DeepTheft achieves SA of 99.01% and LDA of 96.23%. If only BiLSTM is kept, SA and LDA have dropped to 89.88% and 54.45%, respectively. If only UNet is retained, SA and LDA have decreased to 96.57% and 58.16%. If only Temporal-Encoder is removed, SA and LDA becomes 98.32% and 78.19%. If only UPloss is removed, SA and LDA are 98.03% and 83.58%.

9. <https://github.com/FPSG-UIUC/hertzbleed>

Table 8: Inferring performance of the kernel number using direct or indirect regression of $MetaModels_{Hyper}$.

Training Size	Inferring Method	Precision(%)	Recall(%)	F1(%)
50,000 traces	Direct Regression	95.57	91.55	93.28
	Indirect Regression	98.89	98.98	98.93
2,500 traces	Direct Regression	77.58	70.12	72.54
	Indirect Regression	97.02	97.20	97.09

Cross-CPU: Previous experiments are aligned with all existing works’ assumptions where targeted machine configurations (e.g., CPU) are known to an attacker. So that all training energy traces are collected from the same CPU as the targeted machine. We have further collected energy traces from another Intel i7-4710MQ and immediately evaluated it (without transfer learning) with meta-models trained from Intel Xeon-W-2123 (previous experiments are upon Intel Xeon-W-2123). As expected, the SA/LDA becomes 79.79%/59.83% due to energy trace variations across CPUs. To improve the attack performance, we then leverage a few new traces (100 model architectures’ energy traces with five input size per model from Intel i7-4710MQ) to perform transfer learning upon meta-models obtained through Intel Xeon-W-2123. With transfer learning, the SA/LDA has been improved to 99.07%/97.55%.

Noisy Workload: To evaluate the impact of noisy workloads, a third container is created to host a running LAMP (Linux, Apache, MySQL and PHP/Perl/Python) server with its default configuration. It co-resides with two other containers hosting DeepTheft and a victim model respectively. In this setting, 500 energy traces of 100 random architectures (five input-sizes per architecture) are collected as a testing dataset against the training dataset generated in Section 5. As a baseline, in the setting where there is no such noise, another 500 energy traces against the same random architectures are collected. Because of the noise, the pair of SA and LDA has insignificantly dropped to 98.95% and 94.77% compared to the baseline pair of 99.07% and 98.13%.

The accuracy drop is expected to be compensated given repeated queries on the same victim model architecture—note previous DeepTheft performance is upon a single trace snapshot. To this end, we have repeated three times (could be more) on each of 100 different architectures per input size (five input sizes). Algorithms of i) pre-averaging repeated traces and ii) post-majority-voting results are considered. The former improves SA and LDA to 99.03% and 96.68%, respectively. The latter (slightly) outperforms the former, presenting a 99.09% SA and 96.91%.

Threat to Commercial Clouds: Since the RAPL-based power side-channel has been discovered by Lipp et al. [27], unprivileged access to the `powercap` interface in bare-metal OS has been disabled. Despite that, some container-based clouds expose the `powercap` to a container [15], [55]. Based on our experiments, a container, in the latest docker environment of 20.10.18, can access the `powercap` without limitation. Additionally, there exist leading cloud providers that *do* allow a VM to access the RAPL MSRs,

e.g., AWS EC2 reported by Zhang et al. [55].

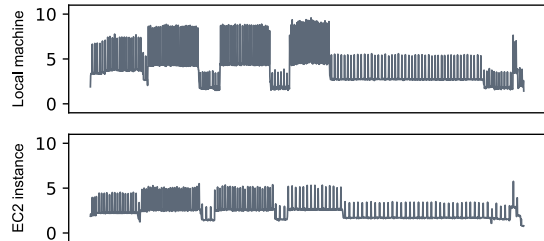


Figure 5: Two energy consumption traces from the DRAM domain are collected for the same model architecture via our experimental local machine (top) and one EC2 instance of c4.8xlarge (bottom).

Following their observation, we have further confirmed that some (not all) EC2 instances have provided access to RAPL. Specifically, some EC2 instances are equipped with a tool called `turbostat` to help monitor the operating state of a processor, such as its frequency, C-state (referring to controlling the sleep levels that a core can enter when it is idle), and P-state (referring to controlling the desired performance in CPU frequency from a core).

More importantly, an EC2 instance can leverage this tool to access RAPL MSRs and thus acquire energy consumption from two domains, i.e., `Package` domain and `DRAM` domain. As AWS provides users with various EC2 instance types, not all of them have provided `turbostat` to access RAPL MSRs. We have experimented with a number of EC2 instances and Table 9 shows whether each instance type supports access to RAPL MSRs. A list of AWS EC2 instances that might enable/disable the RAPL access can be found here¹⁰.

Table 9: Based on our experiments, some AWS EC2 instance types are listed to show whether they are enabled/disabled to access RAPL MSRs.

AWS EC2	Enabled	Disabled
Instance Types	c4.8xlarge, r4.8xlarge, d2.8xlarge, i3.8xlarge, x1e.8xlarge, h1.8xlarge	t1.micro, t2.xlarge, t3.xlarge, c3.2xlarge, c4.2xlarge, c5.2xlarge

On top of that, we pick one instance type of c4.8xlarge to collect the energy trace from the DRAM domain for a given model and compare it with that of our experimental local machine in Section 5, results of which are shown in Figure 5. As can be seen from this figure, their energy traces are similar to each other in terms of their trace shapes, indicating that DeepTheft, running within an EC2 instance, supports the RAPL access, can steal a targeted model architecture running within another EC2 instance. To be specific, for an instance running model inference from an unknown model, DeepTheft can collect its energy consumption traces from another instance. We note that both instances are assumed to

10. https://docs.aws.amazon.com/AWSEC2/latest/UserGuide/processor_state_control.html

co-reside in the same physical machine and only the instance running DeepTheft needs access to RAPL MSRs.

Mitigation: First, limiting container-level access to the RAPL interface can mitigate the power side-channel utilized by DeepTheft. Second, disabling either Turbo Boost or SpeedStep/Hardware Controlled Performance States from the BIOS can mitigate the frequency side-channel exploited by DeepTheft. However, given that our learning-framework is generic to time-series side-channel signals (low sampling rate in particular) besides the validated power and frequency side-channels, more general side-channel mitigation techniques such as masking hardware protection and randomization (e.g., noise injection) are demanded and can be incorporated during the model inference.

As for masking, it divides sensitive information into multiple shares. One of the primary assumptions in masking is that the leakage of each share is independent of the other shares. A successful attack by utilizing the leakage from a single share cannot be performed unless the leakage information from all of the shares is available. Effectively incorporating masking into model inference is an interesting future work. Injecting delicate heavy background noise (e.g., one common means of randomization) is a common approach to reducing the signal-to-noise ratio (SNR) to mitigate side-channel attacks. We have evaluated this by significantly increasing CPU workload: a stress command (`stress -m 8 --vm-bytes 1G`) has been utilized to induce high system noise. Consequently, the SA/LDA decreases from 99.26%/99.75% to 71.28%/46.71%. However, we note that repeated measurements can enhance the SNR, effectively reducing the injected noise.

7. Conclusion

DeepTheft is a new end-to-end model architecture stealing attack that leverages time-series side-channel signals (e.g., power and CPU frequency are used in our paper) in the MLaaS setting. Given the constraint of a low sampling rate, we proposed a new and generic supervised-learning framework that consists of a set of meta-models, i.e., *MetaModel_{Stru}* and *MetaModels_{Hyper}*, based on which DeepTheft can recover a complete network structure and layer-wise hyperparameters. Our extensive experiments have validated the DeepTheft's high efficacy in both model structure topology recovery and layer-wise hyperparameters inferring under a low sampling rate.

References

- [1] ALIBABA CLOUD. ECS Bare Metal Instance Types. <https://www.alibabacloud.com/help/en/elastic-compute-service/latest/ecs-bare-metal-instance-types-overview>, 2023.
- [2] AMAZON, INC. Amazon machine learning. <https://aws.amazon.com/machine-learning>, 2018.
- [3] AMAZON, INC. AWS CPU Inference. <https://docs.aws.amazon.com/deep-learning-containers/latest/devguide/deep-learning-containers-eks-tutorials-cpu-inference.html>, 2018.
- [4] AMAZON, INC. AWS Deep Learning Containers. <https://docs.aws.amazon.com/deep-learning-containers/latest/devguide/deep-learning-containers-ec2-tutorials-inference.html>, accessed: 11-Oct-2022.
- [5] ATYA, A. O. F., QIAN, Z., KRISHNAMURTHY, S. V., LA PORTA, T., MCDANIEL, P., AND MARVEL, L. Malicious co-residency on the cloud: Attacks and defense. In *INFOCOM* (2017), pp. 1–9.
- [6] BALLE, B., CHERUBIN, G., AND HAYES, J. Reconstructing training data with informed adversaries. In *S&P* (2022), IEEE Computer Society, pp. 1556–1556.
- [7] BATINA, L., BHASIN, S., JAP, D., AND PICEK, S. CSI NN: Reverse engineering of neural network architectures through electromagnetic side channel. In *Usenix Security* (2019), pp. 515–532.
- [8] CARLINI, N., CHIEN, S., NASR, M., SONG, S., TERZIS, A., AND TRAMER, F. Membership inference attacks from first principles. In *S&P* (2022), IEEE, pp. 1897–1914.
- [9] CARLINI, N., JAGIELSKI, M., AND MIRONOV, I. Cryptanalytic extraction of neural network models. In *CRYPTO* (2020).
- [10] CHMIELEWSKI, Ł., AND WEISSBART, L. On reverse engineering neural network implementation on GPU. In *ACNS* (2021).
- [11] DOCKER, INC. Home - Docker. <https://www.docker.com/>, 2013.
- [12] EZHILCHELVAN, P. D., AND MITRANI, I. Evaluating the probability of malicious co-residency in public clouds. *IEEE Transactions on Cloud Computing* (2015).
- [13] FREDRIKSON, M., JHA, S., AND RISTENPART, T. Model inversion attacks that exploit confidence information and basic countermeasures. In *Proc. CCS* (2015).
- [14] GANJU, K., WANG, Q., YANG, W., GUNTER, C. A., AND BORISOV, N. Property inference attacks on fully connected neural networks using permutation invariant representations. In *Proc. CCS* (2018), pp. 619–633.
- [15] GAO, X., GU, Z., KAYAALP, M., PENDARAKIS, D., AND WANG, H. Containerleaks: Emerging security threats of information leakages in container clouds. In *DSN* (2017).
- [16] GOOGLE. CPU platforms. <https://cloud.google.com/compute/docs/cpu-platforms>, 2023.
- [17] GOOGLE, INC. Cloud ml engine overview. <https://cloud.google.com/ml-engine/docs/technical-overview>, 2018.
- [18] GRAVES, A., FERNÁNDEZ, S., GOMEZ, F., AND SCHMIDHUBER, J. Connectionist temporal classification: labelling unsegmented sequence data with recurrent neural networks. In *Proc. ICML* (2006), pp. 369–376.
- [19] GRAVES, A., FERNÁNDEZ, S., AND SCHMIDHUBER, J. Bidirectional LSTM networks for improved phoneme classification and recognition. In *ICANN* (2005), pp. 799–804.
- [20] GULIANI, A., AND SWIFT, M. M. Per-application power delivery. In *EUROSYS* (2019), pp. 1–16.
- [21] HAZELWOOD, K., BIRD, S., BROOKS, D., CHINTALA, S., DIRIL, U., DZHULGAKOV, D., FAWZY, M., JIA, B., JIA, Y., KALRO, A., ET AL. Applied machine learning at facebook: A datacenter infrastructure perspective. In *HPCA* (2018), pp. 620–629.
- [22] HE, K., ZHANG, X., REN, S., AND SUN, J. Deep residual learning for image recognition. In *Proc. CVPR* (2016), pp. 770–778.
- [23] HU, X., LIANG, L., LI, S., DENG, L., ZUO, P., JI, Y., XIE, X., DING, Y., LIU, C., SHERWOOD, T., ET AL. Deepsniffer: A DNN model extraction framework based on learning architectural hints. In *ASPLOS* (2020), pp. 385–399.
- [24] HUA, W., ZHANG, Z., AND SUH, G. E. Reverse engineering convolutional neural networks through side-channel information leaks. In *DAC* (2018), pp. 1–6.

- [25] LIANG, S., ZHAN, Z., YAO, F., CHENG, L., AND ZHANG, Z. Clairvoyance: Exploiting far-field EM emanations of GPU to “see” your DNN models through obstacles at a distance. In *IEEE S&P Workshops* (2022), pp. 312–322.
- [26] LIPP, M., GRUSS, D., AND SCHWARZ, M. Amd prefetch attacks through power and time. In *USENIX Security* (2022).
- [27] LIPP, M., KOGLER, A., OSWALD, D., SCHWARZ, M., EASDON, C., CANELLA, C., AND GRUSS, D. Platypus: Software-based power side-channel attacks on x86. In *S&P* (2021), pp. 355–371.
- [28] MAIA, H. T., XIAO, C., LI, D., GRINSPUN, E., AND ZHENG, C. Can one hear the shape of a neural network? snooping the GPU via magnetic side channel. In *Usenix Security* (2022).
- [29] MEYERS, V., GNAD, D., AND TAHOORI, M. Reverse engineering neural network folding with remote FPGA power analysis. In *IEEE Annual International Symposium on Field-Programmable Custom Computing Machines* (2022), pp. 1–10.
- [30] NAGHIBIOUYBARI, H., NEUPANE, A., QIAN, Z., AND ABU-GHAZALEH, N. Rendered insecure: Gpu side channel attacks are practical. In *CCS* (2018), pp. 2139–2153.
- [31] OLIYNYK, D., MAYER, R., AND RAUBER, A. I know what you trained last summer: A survey on stealing machine learning models and defences. *arXiv preprint arXiv:2206.08451* (2022).
- [32] RAKIN, A. S., CHOWDHURY, M. H. I., YAO, F., AND FAN, D. DeepSteal: Advanced model extractions leveraging efficient weight stealing in memories. In *S&P* (2022), pp. 1157–1174.
- [33] RIBEIRO, M., GROLINGER, K., AND CAPRETZ, M. A. Mlaas: Machine learning as a service. In *ICMLA* (2015), pp. 896–902.
- [34] RISTENPART, T., TROMER, E., SHACHAM, H., AND SAVAGE, S. Hey, you, get off of my cloud: exploring information leakage in third-party compute clouds. In *CCS* (2009), pp. 199–212.
- [35] RONNEBERGER, O., FISCHER, P., AND BROX, T. U-net: Convolutional networks for biomedical image segmentation. In *MICCAI* (2015), pp. 234–241.
- [36] SANDLER, M., HOWARD, A., ZHU, M., ZHMOGINOV, A., AND CHEN, L.-C. Mobilenetv2: Inverted residuals and linear bottlenecks. In *Proc. CVPR* (2018), pp. 4510–4520.
- [37] SAROOD, O., LANGER, A., KALÉ, L., ROUNTREE, B., AND DE SUPINSKI, B. Optimizing power allocation to CPU and memory subsystems in overprovisioned HPC systems. In *IEEE International Conference on Cluster Computing* (2013), pp. 1–8.
- [38] SHOKRI, R., STRONATI, M., SONG, C., AND SHMATIKOV, V. Membership inference attacks against machine learning models. In *S&P* (2017), pp. 3–18.
- [39] SIMONYAN, K., AND ZISSERMAN, A. Very deep convolutional networks for large-scale image recognition. *arXiv preprint arXiv:1409.1556* (2014).
- [40] TAN, M., AND LE, Q. Efficientnet: Rethinking model scaling for convolutional neural networks. In *ICML* (2019), PMLR, pp. 6105–6114.
- [41] TIAN, S., MOINI, S., WOLNIKOWSKI, A., HOLCOMB, D., TESSIER, R., AND SZEFER, J. Remote power attacks on the versatile tensor accelerator in multi-tenant FPGAs. In *FCCM* (2021), pp. 242–246.
- [42] TRAMÈR, F., ZHANG, F., JUELS, A., REITER, M. K., AND RISTENPART, T. Stealing machine learning models via prediction APIs. In *Usenix Security* (2016), pp. 601–618.
- [43] VARADARAJAN, V., ZHANG, Y., RISTENPART, T., AND SWIFT, M. A placement vulnerability study in {Multi-Tenant} public clouds. In *Usenix Security* (2015), pp. 913–928.
- [44] WANG, B., AND GONG, N. Z. Stealing hyperparameters in machine learning. In *S&P* (2018), IEEE, pp. 36–52.
- [45] WANG, Y., PACCAGNELLA, R., HE, E. T., SHACHAM, H., FLETCHER, C. W., AND KOHLBRENNER, D. Hertzbleed: Turning power side-channel attacks into remote timing attacks on x86. In *USENIX Security* (2022), pp. 679–697.
- [46] WEI, J., ZHANG, Y., ZHOU, Z., LI, Z., AND AL FARUQUE, M. A. Leaky DNN: Stealing deep-learning model secret with GPU context-switching side-channel. In *DSN* (2020), pp. 125–137.
- [47] WEI, L., LUO, B., LI, Y., LIU, Y., AND XU, Q. I know what you see: Power side-channel attack on convolutional neural network accelerators. In *ACSAC* (2018), pp. 393–406.
- [48] WOLF, S., HU, H., COOLEY, R., AND BOROWCZAK, M. Stealing machine learning parameters via side channel power attacks. In *IEEE Computer Society Annual Symposium on VLSI* (2021), pp. 242–247.
- [49] XIANG, Y., CHEN, Z., CHEN, Z., FANG, Z., HAO, H., CHEN, J., LIU, Y., WU, Z., XUAN, Q., AND YANG, X. Open DNN box by power side-channel attack. *IEEE Transactions on Circuits and Systems II: Express Briefs* (2020), 2717–2721.
- [50] YAN, M., FLETCHER, C. W., AND TORRELLAS, J. Cache telepathy: Leveraging shared resource attacks to learn DNN architectures. In *Usenix Security* (2020), pp. 2003–2020.
- [51] YU, H., MA, H., YANG, K., ZHAO, Y., AND JIN, Y. DeepEM: Deep neural networks model recovery through EM side-channel information leakage. In *HOST* (2020), pp. 209–218.
- [52] ZHANG, H., AND HOFFMANN, H. Maximizing performance under a power cap: A comparison of hardware, software, and hybrid techniques. In *ASPLOS* (2016), pp. 545–559.
- [53] ZHANG, Y., JUELS, A., REITER, M. K., AND RISTENPART, T. Cross-tenant side-channel attacks in paas clouds. In *CCS* (2014), pp. 990–1003.
- [54] ZHANG, Y., YASAEI, R., CHEN, H., LI, Z., AND AL FARUQUE, M. A. Stealing neural network structure through remote FPGA side-channel analysis. *IEEE Transactions on Information Forensics and Security* (2021), 4377–4388.
- [55] ZHANG, Z., LIANG, S., YAO, F., AND GAO, X. Red alert for power leakage: Exploiting intel rapl-induced side channels. In *Proc. AsiaCCS* (2021), pp. 162–175.
- [56] ZHU, Y., CHENG, Y., ZHOU, H., AND LU, Y. Hermes attack: Steal DNN models with lossless inference accuracy. In *Usenix Security* (2021).

Appendix A. Domain Knowledge

As shown in Table 2, only three layer types have different layer-wise hyperparameters. In the following, we introduce all these layer-wise hyperparameter and their correlations based on the domain knowledge of popular and complex network families (e.g., MLP, AlexNet, VGG and ResNet), aligned with the SOTA [28].

A Convolutional Layer: This layer can have 7 hyperparameters, i.e., C_{in} , C_{out} , K , S , P , D , and G , which are introduced below:

- C_{in} is the number of channels of an input. For the first layer, it is known as 1 or 3 dependent on whether an input image is grey or color. For other layers, C_{in} is the same as C_{out} of a preceding layer, indicating C_{in} can be decided when its preceding layer’s C_{out} is known.
- C_{out} is the channel number of an output feature map, equaling to the number of convolutional kernels. It is often selected from a wide range of discrete integer values. Generally, C_{out} is set based on some heuristics. For example, C_{out} of popular networks such as VGG and ResNet is set to be 2^n where n can be from $\{4, 5, 6, \dots\}$.

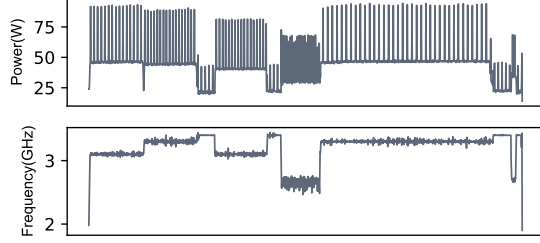


Figure 6: Time-series traces extracted from the RAPL-based power side channel (top) and DVFS-enabled CPU frequency side channel (bottom), respectively. While they look different to each other, our proposed learning framework can learn each correlation between the time-series traces and DNN model architectures in the offline phase and achieves high attack performance in the online phase.

- K is the size of a convolutional kernel, which is often an odd number. Generally, K does not exceed 7 [28].
- S is the stride, indicating the amount of movement when a convolutional kernel moves. By default, it is set to 1 by default or 2 if the convolutional kernel is used to perform downsampling.
- P is the size of padding, which is often added to the edges of feature maps to allow for more space for a convolutional kernel to cover the feature maps. By default, $P = \lfloor (K - 1)/2 \rfloor \times D$, with D as the dilation.
- D is the space between kernel elements and G is the number of blocked connections from the input channel to the output channel. By default, D and G are 1 for a classification task. Generally, $D \neq 1$ is used in semantic segmentation networks, and $G \neq 1$ is used in lightweight networks, e.g., tiny machine learning on edge devices. Thus, both D and G are 1 in our target model architectures.

A MaxPooling Layer: This layer can have 4 hyperparameters, i.e., K , S , P and D , which have similar meanings to that of the convolutional layer but different values. Specifically, K is picked from $\{2, 3\}$. S is from $\{1, 2\}$. P is from $\{0, 1\}$. D is set to 1.

A Linear Layer: This layer can have 2 hyperparameters, i.e., F_{in} and F_{out} . Specifically, F_{in} is the input-feature size. Similar to C_{in} , its value can be decided by C_{out} or F_{out} . F_{out} is the output-feature size that is either equal to the number of classes in the last linear layer, or 2^n where n can be $\{4, 5, 6, \dots\}$ for other linear layers.

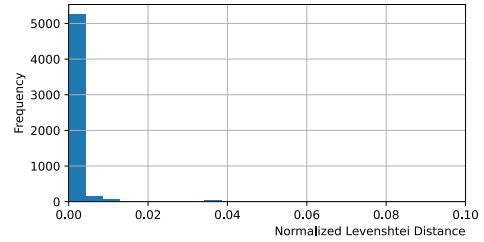


Figure 7: A distribution of normalized Levenshtein distances on the testing dataset of 5,760 energy traces. 0 means an exact network-structure match.